Research Article

Nano Research
2023, 16(7): 10652–10659

ISSN 1998-0124 CN 11-5974/O4
https://doi.org/10.1007/s12274-023-5634-x

Highly selective adsorption of light hydrocarbons in a HKUST-like MOF constructed from spirobifluorene-based octacarboxylate ligand by a substitution strategy

Xinli Shi, Yucong Zu, Xilin Li, Tongyi Zhao, Hao Ren, and Fuxing Sun (✉)

State Key Laboratory of Inorganic Synthesis and Preparative Chemistry, Jilin University, Changchun 130012, China

Received: 15 November 2022 / **Revised:** 13 February 2023 / **Accepted:** 2 March 2023

ABSTRACT

Metal-organic frameworks (MOFs) with HKUST-like **tbo** structures have been paid specific attention for gas sorption and separation because of their specific pore features. According to the geometric similarity of spirobifluorene and $[Cu_2(O_2CR)_4]$ paddlewheel secondary building units (Cu2 SBUs) in HKUST-1, we attempted to rationally construct a HKUST-like MOF by a substitution strategy. Using a judiciously designed octatopic carboxylate ligand, a copper-organic framework, JUC-220, was synthesized. The crystals of JUC-220 exhibited characteristic features in cubic with disorder, possibly due to the disorder substitution and high symmetry of **tbo** topology. Two related HKUST-like structure models were considered. Thanks to the suitable pore size and specific pore shapes, the adsorption selectivities of JUC-220 for C_3H_8/CH_4 (5/85) and C_2H_6/CH_4 (10/85) gas mixtures were as high as 736 and 46 respectively at 298 K and 1 bar. Specially, JUC-220 exhibited excellent trace adsorption performance of C_3H_8 and C_2H_6 as well as reverse adsorption behavior of C_2H_6/C_2H_4. Thus, JUC-220 serves as an example of HKUST-like MOF with disorder for light hydrocarbons separation and the implementation of substitution which can be used to explore more porous MOFs.

KEYWORDS

HKUST-like metal-organic frameworks (MOFs), reticular chemistry, disorder, substitution, trace adsorption, light hydrocarbons separation

1 Introduction

Metal-organic frameworks (MOFs) are crystalline microporous materials self-assembled from metal ions or clusters and organic ligands with various topological nets [1]. Owing to their high surface areas and crystallinity, as well as their tunable pore features (size, shape, and inner surface with adsorption sites), MOFs have been intensively explored for gas storage and separations [2, 3]. Meanwhile, reticular chemistry is an attractive and effective tool to synthesize MOFs with desired structures or properties [4, 5]. However, the rational construction of targeted MOFs remains a substantial challenge, especially by highly connected organic linkers (e.g., with 6–8 connectors) [6]. Firstly, the highly connected organic linkers are usually difficult to synthesize because they have larger molecular volume and weight with more branches and coordinating groups. Secondly, the large molecular volume and weight of highly connected organic ligands usually brings a dissolution problem when using them to assemble MOFs under solvothermal method. Lastly, the biggest challenge is that the structure of highly connect organic ligands in solution is more flexible and harder to control during MOF formation because of their rotatable multi-branches. All these drawbacks could lead to the difficulty of crystallization of regular MOFs and prevent us from the structural solution of MOFs by single-crystal X-ray diffraction (XRD) [7, 8]. On the other hand, MOFs exhibiting interesting types of structural disorder, including topological disorder, static disorder, dynamic disorder, and low-dimensional disorder, are attracting increasing attention owing that they offer a platform to understand the formation of these complex disorder structures and also whether it might be implicated in useful functionalities [9, 10].

The separation of light hydrocarbons, especially C1-3 hydrocarbons, is very challenging and relies almost exclusively on high-pressure cryogenic distillation because of their low boiling points and small molecular sizes [3]. Adsorption-based methods based on selective adsorption by the adsorbent, usually porous solids, could replace the thermally driven separation techniques, and significantly reduce the energy consumption as well as the cost of manufacturing these common important chemicals. The properties of solid adsorbents (composition, surface polarity, pore structure, etc.) manifestly play a key role in this developing technology and largely determine the final separation efficiency. Among a large amount of research on MOFs focusing on the storage and separation of light hydrocarbons, MOFs with **tbo** topology (the canonical HKUST-1 firstly [11]) constructed with $[Cu_2(O_2CR)_4]$ paddlewheel secondary building units (Cu2 SBUs) and multicarboxylate ligands have been paid specific attention mainly because of their specific porous frameworks with two kinds of cages and open metal sites. HKUST-1 was reported as a good benchmarking compound for CH_4 sorption at ambient conditions [12], and firstly examined for C_2H_4/C_2H_6 separation

Address correspondence to fxsun@jlu.edu.cn

[13]. One of HKUST-like tbo-MOFs, Cu-tbo-MOF-5 was reported in 2016 to behave the best performing CH_4 storage among all the MOFs at that time [14]. In contrast to other MOFs with exposed metal sites for CH_4 adsorption, HKUST-1 and HKUST-like MOFs have additional strong adsorption sites located in the windows of each octahedral cage owing to several close interactions to CH_4 matched with suitable distances and symmetries [14–16].

To synthesize HKUST-like MOFs rationally, Eddaoudi et al. used a pillaring strategy which they called the supramolecular building layer (SBL) approach through the deconstruction of **tbo** topology into the edge-transitive (4,4)-connected square lattice (**sql**) cross-linked through quadrangular pillars (Fig. S1 in the Electronic Supplementary Material (ESM)) [17]. The underlying layer could be designed as Cu2 SBUs bridged by isophthalate ligands, and thus quadrangular-core tetraisophthalate ligands were designed and used to access three tbo-MOFs. Subsequently, Schröder et al. reported the challenging syntheses of a series of isoreticular octacarboxylate MOFs, MFM-180 to -185, by varying the length and nature of the quadrangular cores of the tetraisophthalate linkers [18]. These MOFs are with effective modulation of porosity and high performance of CH_4 storage. What's more, the reduction of Cu2 SBUs in the structure of HKUST-like MOF would increase its stability against water humidity, such as BUT-155 constructed from Cu(II) and an octacarboxylate ligand with six methyl groups showing exceptional hydrolytic stability [19]. Very recently, Li, B. and Chen, B. L. et al. reported another HKUST-like MOF ZJU-50a, which also exhibits high water stabilities as well as high density of supramolecular binding sites for both high C_2H_2 storage and selectivity [20].

Herein, we designed and synthesized a new octatopic carboxylic ligand with central spirobifluorene (SBF) core and four isophthalate branches, namely 5,5',5'',5'''-(9,9'-spirobi[fluorene]-2,2',7,7'-tetrayl)tetraisophthalic acid (H_8SFTTP). The synthetic procedures of H_8SFTTP were shown (Section S3.1 in the ESM). The SBF-core is with very specific rigid geometry, constituted of two orthogonal fluorene units connected through a shared spiro carbon. Therefore, it could be designed as 4-connected (4-c) square node with phenyl rings perpendicular to the square [21], which is different from other 4-c square ligands [22, 23]. Furthermore, we notice that the geometry and size of SBF are highly similar to the classic Cu2 SBUs in HKUST-1(Fig. S2 in the ESM). We conceived that this octatopic ligand could form a framework with a portion of inorganic Cu2 SBUs in HKUST-1 replaced by the organic segment SBFs, since we had done a similar replacement in the case of JUC-100 based on the classic MOF-5 [24]. Using the ligand H_8SFTTP, we synthesized a copper-organic framework (named JUC-220, JUC = Jilin University, China) (Scheme 1). The crystals of JUC-220 were revealed to be twins or/and polymorphs in cubic, and two possible HKUST-like phases in JUC-220 were considered. The potential use of JUC-220 for gas separation was investigated, which demonstrated that JUC-220 exhibited highly selective gas adsorption performance of C_3H_8/CH_4 and C_2H_6/CH_4 as well as trace adsorption performance of C_3H_8 and C_2H_6.

2 Results and discussion

SBF and its derivatives have been reported as chiral ligands and electropolymerizable building blocks, and they play a key role in the development of biomedicine, organic electronics, and solid-state laser [25]. However, the use of SBF-core ligands for the synthesis of crystalline porous MOFs attracted more attention only in recent few years [26–32]. And there are only no more than

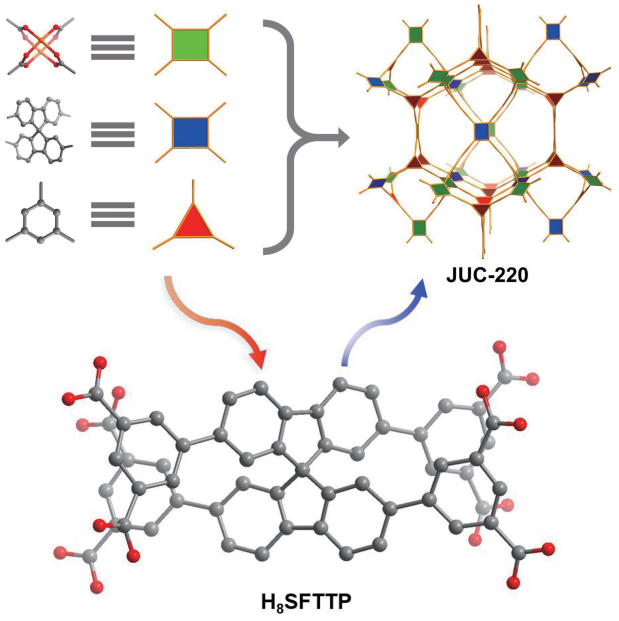

Scheme 1 The construction strategy of a HKUST-like MOF by substitution in this work.

fifty coordination polymers reported based on SBF-core ligands, although few them showed permanent porosity and the number of structures in the MOF subset of the Cambridge Structural Database (CSD) is over 110,000 [33], probably because of the low crystallization ability of SBF-based compounds. On the other side, SBF-based monomers have been reported for the synthesis of porous organic polymers for optoelectronic applications and gas separation [34–37]. In this work, the key motivation for design of the dendritic ligand H_8SFTTP is the geometric similarity of SBF and the Cu2 SBUs in HKUST-1, thus to obtain a HKUST-like framework by substitution and modified pore environment for gas separation.

To implement our design strategy, solvothermal reaction between H_8SFTTP and $Cu(NO_3)_2{\cdot}3H_2O$ in a mixed solvent of N,N'-dimethylformamide (DMF) and ammonia solution was performed. The reaction yielded a homogeneous crystalline material JUC-220. Optical microscopy and scanning electron microscopy (SEM) demonstrate that JUC-220 exhibits uniform rhombic dodecahedral morphology which is for typical cubic crystals expressing {110} crystal facets (Figs. 1(a) and 1(b)) [38]. The crystals were green and with size from several micrometers to around 100 micrometers. Sequentially, we attempted to solve the structure by single crystal X-ray diffraction. The diffraction patterns provided strong and periodic spots indicating the high crystallinity of JUC-220 (Fig. 1(c) and Fig. S6 in the ESM). The spots are clear and appear to be without any elongation, indicating the crystal is not badly splitting. After three-dimensional (3D) reciprocal lattice was constructed, the indexing of observed reflections identified a body-centered cubic Bravais lattice with two dominant domains and gave a unit cell with $a = b = c =$ 35.87 Å (Fig. 1(d) and Figs. S7 and S8 in the ESM). But next, we had a serious problem when reducing and integrating the diffraction data, since the average correlation coefficient values of spot shape were very low which means that most of the spots were not perfect sphere and many reflections observed were overlapped, suggesting the intrinsic property of twinning in JUC-220 (Fig. S9 in the ESM). Moreover, the complexity of twinning on cubic crystals in crystallography prevented us from a successful structure solution [8, 39]. The polymorphism of JUC-220 might arise from the quasi-planar SBF core which is with pseudo high symmetry as the Cu2 SBUs or/and the similar but different

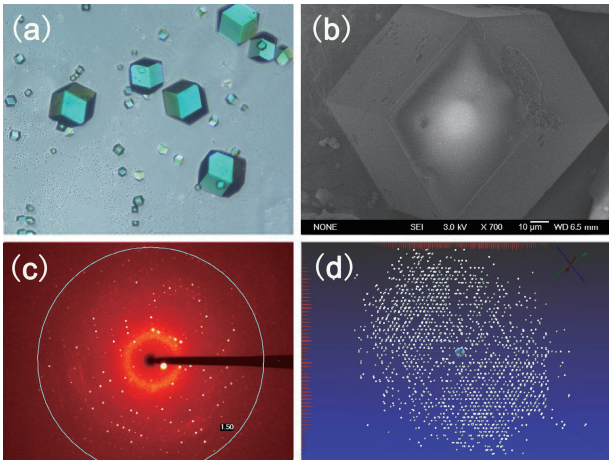

Figure 1 (a) Optical image and (b) SEM image of JUC-220 crystals. (c) A frame of single-crystal X-ray diffraction for JUC-220. (d) Reconstructed 3D reciprocal lattice of JUC-220.

geometrical size of SBF core to Cu2 SBUs, thus leading to some degree of disorder in the substitution of organic segments for inorganic SBUs.

To elucidate the structure, we noticed that the unit cell parameters of JUC-220 correlate with that of some tbo-MOFs, such as MFM-180 ($a = b = 18.69$ Å, $c = 35.9$ Å; space group: $I\bar{4}2m$) [18]. What's more, the unit cell length of 35.87 Å for JUC-220 approximates to the [110] period of the cubic HKUST-1 structure. Considering the reason for the design of H_8SFTTP mentioned above, we constructed two structural models based on the structure of HKUST-1. It is worth mentioning that all the reported HKUST-like MOFs based on Cu2 SBUs and tetraisophthalate linkers are with the same topology to tbo-MOFs by Eddaoudi et al. so far. This kind of binodal **tbo**-derived net can transform to **scu** topology if the linkers are regarded as 8-c nodes (Figs. 2(a) and 2(c)). During our quest, we recognized that the replacement of Cu2 SBUs in HKUST-1 by organic segments in our strategy could also lead to another binodal **tbo**-derived net, which could transform to another (4,8)-c net **urj** topology when the linkers act as 8-c nodes (Figs. 2(b) and 2(d)). Based on these two binodal **tbo**-derived nets and with the help of unit cell parameters obtained from single crystal X-ray diffraction, we generated the structural models, JUC-220-scu and JUC-220-urj (Figs. 2(e) and 2(f) respectively). These two isomeric structures are both in tetragonal crystal system, but different space groups ($I\bar{4}2m$ for JUC-220-scu and $P\bar{4}n2$ for JUC-220-urj respectively). These structure models were geometrically optimized and both of them exhibited reasonable assembly of Cu2 SBUs and SFTTP linkers. It is supposed that the crystals of JUC-220 were twins or/and polymorphs of several domain states including JUC-220-scu, JUC-220-urj or/and other unexpected ones.

The phase of JUC-220 was characterized by powder X-ray diffraction (PXRD). As shown in Fig. 3(a), the experimental PXRD pattern of as-synthesized JUC-220 sample shows characteristic peaks. And then, we tried to index the peaks based on the lattice information obtained from single-crystal diffraction. It is found that the space group $Ia\bar{3}d$ (no. 230) is mostly in accordance with the existing peaks in the PXRD pattern (Fig. S13 in the ESM). The signals at 6.92°, 9.18°, 9.8°, 12.02°, 15.9°, 17.8°, and 19.38° correspond to the (220), (321), (400), (422), (541), (640), and (732) crystal planes. However, there are still few peaks which don't agree with the lattice, including two small peaks at 6.4° and 6.56° as well as the strong peak at 11.8° which is very close to the peak at 12.02°, demonstrating the disorder in the structure of JUC-220. Subsequently, we compared the PXRD pattern of JUC-220 with the simulated patterns of HKUST-1, JUC-220-scu,

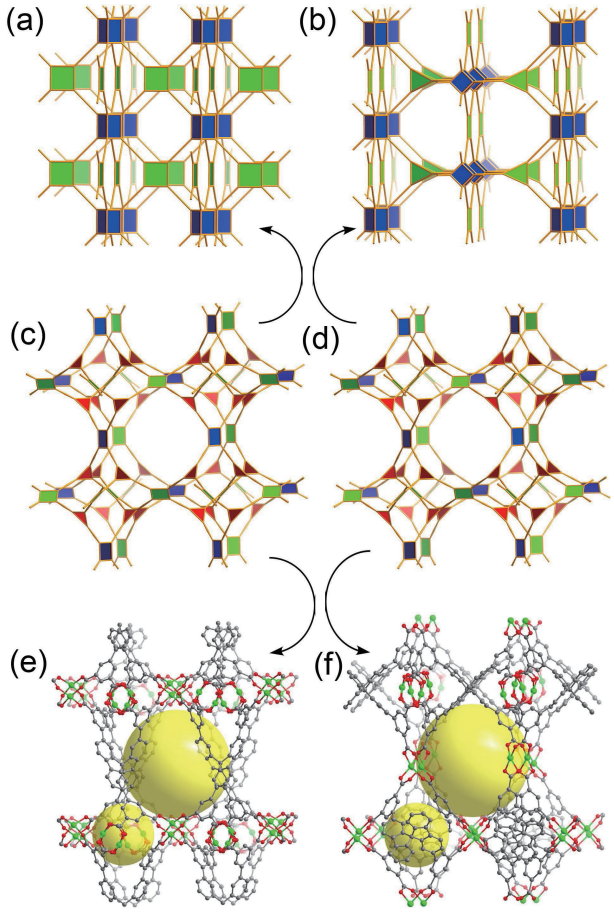

Figure 2 (a) and (c) (4,8)-c nets of **scu** and **urj** topology respectively (blue: 8-c nodes; green: 4-c nodes). (b) and (d) Two kinds of **tbo**-derived nets (green and blue: 4-c square-like nodes; red: 3-c triangle-like nodes). (e) and (f) Modeling structures of JUC-220-scu and JUC-220-urj respectively (green: Cu; red: O; gray: C; yellow balls are used to show the pores).

and JUC-220-urj. As shown in Fig. 3(a), the PXRD pattern of JUC-220 is close to these patterns, especially that of HKUST-1, although their unit cell parameters are not the same. In detail, the diffraction pattern of JUC-220 behaves more peaks than that of HKUST-1 in cubic and fewer peaks than those of JUC-220-scu and JUC-220-urj in tetragonal crystal system, because the number of reflections is prone to decrease with higher symmetry theoretically. The disappearance of some peaks from patterns of JUC-220-scu and JUC-220-urj including the strong peak at ~ 5° in JUC-220 pattern is probably due to the disorder in the framework, diffraction overlap or/and different systematic absences of reflections because of higher pseudo-symmetry in JUC-220. To reveal more structural information, Fourier transform infrared spectroscopy (FT-IR) measurements were performed (Fig. S14 in the ESM). Compared with FT-IR pattern of H_8SFTTP, the pattern of JUC-220 shows that the peaks at ca. 1240 and ca. 3000 cm^{-1} which could be contributed to isolated hydroxyls almost diminished, indicating the deprotonation of the ligands in JUC-220 was accomplished [40].

To access the guest solvents of JUC-220, we implemented thermogravimetric analysis (TGA) for JUC-220. JUC-220 experienced three different stages of weight loss when the temperature gradually increased (Fig. S15 in the ESM). About 25.8 wt.% loss before 340 °C could be contributed to the department of guest DMF and water molecules. And then, the skeleton of JUC-220 began to sharply collapse. The decomposition finished at ca. 400 °C. N_2 sorption isotherm at 77 K for JUC-220 was measured to examine its permanent porosity. Before the measurement, the sample was solvent-exchanged with methanol

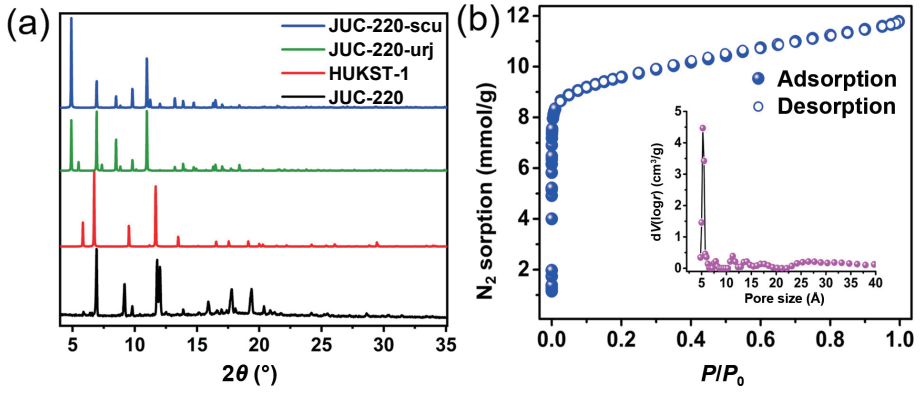

Figure 3 (a) PXRD patterns of as-synthesized JUC-220 and simulated structures. (b) Nitrogen sorption isotherm at 77 K for JUC-220 (insert: the corresponding pore size distribution curve calculated by NLDFT).

and dichloromethane in sequence, and then evacuated at 100 °C for 10 h. As shown in Fig. 3(b), JUC-220 behaves a typical type-I N_2 sorption isotherm as expected for microporous material. The Brunauer–Emmett–Teller (BET) surface area and pore volume were calculated to be 828 m^2/g and 0.375 cm^3/g. Pore size distribution (PSD) was also calculated using non-local density functional theory (NLDFT). The corresponding curve shows a high and narrow peak at 5.3 Å (insert in Fig. 3(b)), which agrees with the window size of simulated structural models. There are also some small and broad peaks on the PSD curve, of which the highest centered at 11.3 Å could correspond to the size of cage in the simulated models and others might origin from the disorder of JUC-220. It should be noted that the surface area of JUC-220 is lower than HKUST-1 and other HKUST-like MOFs. And the PSD of JUC-220 is dominated by the window size while HKUST-1 and other HKUST-like MOFs are mostly dominated by their cage size, which might be caused by its highly twinning structure and lead to the decrease of surface area of JUC-220. In order to explore the stability of JUC-220, we measured the PXRD patterns of JUC-220 after activation and N_2 sorption measurement and the second cycle of N_2 sorption at 77 K (Figs. S16 and S17 in the ESM). It can be seen that after activation and N_2 sorption measurements, the peaks of PXRD patterns at 6.4°, 6.56°, and 11.8° which do not agree to the crystal lattice were diminished, while the peak at 11.06° corresponding to the (420) crystal plane appeared. This phenomenon might indicate that the department of solvents in as-synthesized JUC-220 reduced the disorder in JUC-220 crystals. Almost no change was observed in the comparison of N_2 sorption isotherms, indicating that JUC-220 retained its good crystallinity and porosity. We also checked the PXRD pattern of JUC-220 treated in water for 3 weeks (Fig. S18 in the ESM). The maintenance of key peaks indicated its stability in water.

As the kinetic diameters of C1-3 hydrocarbons and CO_2 which commonly presents in the production and utilization of light hydrocarbons are in the 3–5 Å range, the desirable pore size and intrinsic permanent porosity of JUC-220 promoted us to further investigate its potential application for light hydrocarbons separation. Single-component CH_4, C_2H_6, C_3H_8, C_2H_4, C_2H_2, and CO_2 sorption isotherms for JUC-220 at 298 and 273 K up to 1.0 bar were measured. All the gas adsorptions showed reversible type I isotherms. As shown in Fig. 4(a) and Fig. S19 in the ESM, the adsorption of C_3H_8 and C_2H_6 increases sharply in low pressure region (< 0.05 bar) for both isotherms at 298 and 273 K, while the CH_4 adsorption is low and shows almost linear isotherm. These results indicate that there exists higher adsorption affinity of the JUC-220 skeleton towards C_3H_8 as well as C_2H_6 respectively compared to CH_4. The C_2H_4, C_2H_2, and CO_2 adsorption also showed concave isotherms and higher uptakes compared to CH_4 (Fig. 4(b) and Fig. S20 in the ESM). The C_2H_2 adsorption demonstrated close capacity in contrast to C_2H_6, and both of C_2H_2 and C_2H_6 were higher than that of C_2H_4. It should be noted that the order of gases that MOF materials prefer to adsorb is typically $C_2H_2 > C_2H_4 > C_2H_6$ owing to their decreasing polarity [41]. The C_2H_6-selective adsorption behavior of JUC-220 for C_2H_6/C_2H_4 separation benefits to avoid multi-cycles of adsorption and desorption when producing high purity C_2H_4 which is an important issue in industry.

To quantitatively evaluate the binding strength of examined gases in JUC-220, their isosteric heats of adsorption (Q_{st}) on JUC-220 under various loadings were estimated using the Clausius–Clapeyron equation following fitting of the adsorption isotherm data at 273 and 298 K using a virial equation [42]. The Q_{st} values for CH_4 lie in the range 21.5–23.0 kJ/mol, while for CO_2, C_2H_n (n = 2, 4, 6), and C_3H_8 these values are in the ranges 28.9–30.2, 33.9–39.0, and 41.6–50.1 kJ/mol respectively (Figs. S21–S32 in the ESM). The sequence of the ensuing enthalpies is $C_3H_8 > C_2H_6 \approx C_2H_4 \approx C_2H_2 > CO_2 > CH_4$, which is consistent with a supposable consequence based on the isotherms. Compared to other MOFs, the Q_{st} for CO_2 on JUC-220 is moderate [43], whereas those for alkanes are higher than many reported MOFs such as MFM-202a [44], Fe_2(dobdc) [45], and UTSA-35a [46], compared to BSF-2 [47], SBMOF-2 [48], and ZUL-C1 [49], less than ZUL-C2 [49]. The high binding strength of JUC-220 to alkanes was plausibly owing to the pore features of HKUST-like MOFs offering close and strong interactions to hydrocarbons, and especially their additional triangle windows of octahedral cages could provide special interaction to methyl groups with 3-axis symmetry [16]. It should be noted that the similarity of C_2H_2, C_2H_4, and C_2H_6 enthalpies was possibly due to the trade-off between the effects of suitable pore features of JUC-220 for C_2H_6 adsorption [50] and higher polarity of C_2H_2 and C_2H_4 than C_2H_6 [51].

The efficient separations of $C_3H_8/C_2H_6/CH_4$ are prerequisites for fully utilizing the resources and updating the quality of natural gas [41]. Pipeline natural gas is a hydrocarbons gas mixture, consisting of 70 wt.%–96 wt.% CH_4, 0 wt.%–20 wt.% C_2H_6, 0.01 wt.%–5 wt.% C_3H_8, trace amounts of H_2O, etc. [52]. The achievement of ultrapure CH_4 is highly necessary for the reduction of low emission of CO_2, cost-efficient delivery of CH_4 in pipeline, and efficient conversion of CH_4 into value-added product [41]. Meanwhile, the separated individual C_2H_6 and C_3H_8 gases are widely needed in their cracking processes to generate alkene respectively [41]. The strong adsorption affinities of the pores in JUC-220 towards C_3H_8 based on the above analysis indicate that it could adsorb trace amounts of C_3H_8 from the gas mixture of $C_3H_8/C_2H_6/CH_4$. At 298 K and 0.01, 0.03, and 0.05 bar, the C_3H_8 adsorption capacities for JUC-220 are 1.93, 2.37, and 2.55 mmol/g respectively (Fig. 4(c)), while they are 2.58, 2.86, and 2.99 mmol/g

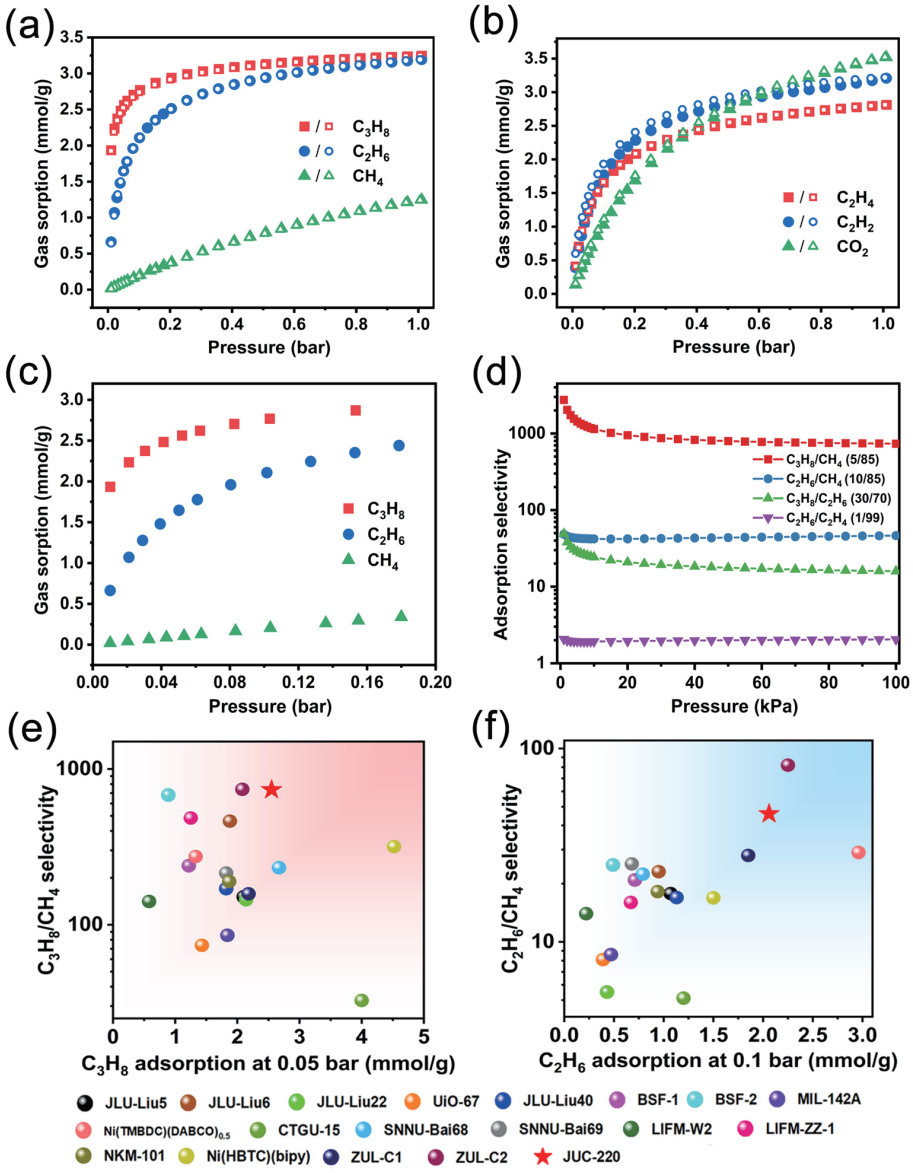

Figure 4 Gas sorption isotherms for (a) CH_4, C_2H_6, and C_3H_8 and (b) CO_2, C_2H_2, and C_2H_4 at 298 K (filled: adsorption; empty: desorption). (c) Gas adsorption isotherms for CH_4, C_2H_6, and C_3H_8 under low pressure and 298 K. (d) Adsorption selectivities using IAST theory for the separation of various gases. (e) and (f) Comparison of the adsorption selectivity and adsorption capacity of C_3H_8 and C_2H_6 under low pressure at 298 K (Table S7 in the ESM).

at 273 K respectively, indicating the high adsorption abilities of JUC-220 for C_3H_8 at low pressure. Compared to C_3H_8 adsorption, the C_2H_6 adsorption for JUC-220 is with relatively weak adsorption affinity, and the C_2H_6 adsorption capacity for JUC-220 is 2.06 mmol/g at 0.1 bar and 298 K, while it is 2.81 mmol/g at 273 K. In harsh contrast, the CH_4 adsorptions for JUC-220 at 0.1 bar are only 0.20 and 0.42 mmol/g at 298 and 273 K respectively. These results may indicate the highly selective C_3H_8 or C_2H_6 adsorptions from CH_4.

The separation performance of C_3H_8, C_2H_6, and CH_4 by JUC-220 was investigated by the calculation of adsorption selectivities using ideal adsorbed solution theory (IAST). The adsorption data of these gases were fitted with the dual-Langmuir–Freundlich isotherm model, while CH_4 adsorption data were fitted with a single-site Langmuir model [45]. As shown in Fig. 4(d), the adsorption selectivities of JUC-220 for C_3H_8/CH_4 (5/85) and C_2H_6/CH_4 (10/85) gas mixtures were as high as 736 and 46 respectively at 298 K and 1 bar. It is worth noting that these values are both higher than all existing MOFs under the same condition except the polycycloalkane-carboxylate MOF, ZUL-C2 [53], which was reported very recently (Fig. 4(e) and Table S7 in the ESM). We also calculated the adsorption selectivities of equimolar C_3H_8/CH_4 and C_2H_6/CH_4 at 298 K for JUC-220 which are 873 and 39 respectively and compared to more reported MOFs (Table S8 in the ESM). It was found that the C_3H_8/CH_4 selectivity is higher than most reported MOFs under the same condition, such as JUC-100 to -103 [54], Mg-MOF-74 [15], UiO-67 [55], FIR-C1 [56], and JLU-MOF51 [57] with large pores, UTSA-35a [46], MOF-801 [58], FJI-C4 [59], SNNU-Bai68 [52], and JLU-Liu21 [60] with small pores, and even BSF-1 [61] with free anions, compared to JLU-Liu40 [62], only lower than BSF-2 [47], MIL-142A [63], and Ni(HBTC)(bipy) [64]. Meanwhile, the C_2H_6/CH_4 selectivity of JUC-220 is also higher than most reported MOFs, only lower than BSF-2 [47] and ZUL-C2 [53], and compared to FJI-C4 [59] (Table S8 in the ESM). The C_3H_8/C_2H_6 (30/70) selectivity for JUC-220 at 298 K was also calculated to be 15.9 at 1 bar which is higher than SNNU-Bai68 (9.2) [52] and SNNU-Bai69 (6.8) [65]. These results indicate that JUC-220 is one of the benchmark materials for alkane separation. It is worth noting that HKUST-1, tbo-MOF-2, and tbo-MOF-3 were also reported to have the abilities of selectively adsorbing C_2H_6 or C_3H_8 from CH_4 which are moderate in MOFs, although they have large pore sizes (Table S8 in the ESM) [15, 66]. Therefore, the outstanding selective adsorption of C_3H_8 or C_2H_6 from CH_4 for JUC-220 was probably owing to its

pore feature of HKUST-like structure and suitable pore size. In order to properly examine the potential of JUC-220 for adsorptive separations of these light hydrocarbons in pressure swing adsorption (PSA) devices, breakthrough calculations were performed with an equimolar C_2H_6/CH_4 and C_3H_8/CH_4 mixture in an adsorber bed packed respectively, using the methodology described in earlier publications [67–71]. The results showed that JUC-220 has significantly high production capacities for use in practice (Fig. S41 in the ESM). Furthermore, we also calculated the adsorption selectivities of JUC-220 for equimolar gas mixtures of C_2H_6/C_2H_4, C_2H_2/C_2H_4, and C_2H_2/CO_2 at 298 and 273 K (Figs. S39 and S40 in the ESM) as well as the gas mixture of C_2H_6/C_2H_4 with 1/99 ratio. The adsorption selectivities of C_2H_6/C_2H_4 (1/99 and 50/50) at 298 K were 2.05 and 2.1 respectively (Fig. 4(d) and Fig. S39 in the ESM), indicating its separation ability of C_2H_6 from C_2H_4.

3 Conclusions

In conclusion, according to the geometric similarity of SBF and Cu2 SBUs in HKUST-1, we designed a HKUST-like MOF by substitution of inorganic clusters for organic segments, and synthesized a copper-organic framework, JUC-220. The crystals of JUC-220 showed characteristic features in cubic with disorder, possibly due to the disorder substitution and high symmetry of **tbo** topology. The novel tbo-MOF exhibited permanent porosities and micropores with prominent pore size around 5.3 Å. Gas sorption behavior of JUC-220 for CH_4, C_2H_6, C_3H_8, C_2H_4, C_2H_2, and CO_2 was studied. The results showed that JUC-220 has highly selective gas adsorption abilities for $C_3H_8/C_2H_6/CH_4$. In addition, JUC-220 exhibited trace adsorption of C_3H_8/C_2H_6 and reverse adsorption behavior of C_2H_6/C_2H_4 at room temperature. Future work will include the characterization for more structural information of JUC-220 as well as more instances of the substitution strategy since the paddlewheel SBUs are common in the structure of porous MOFs for gas storage and separation.

Acknowledgements

This research work was supported by the National Natural Science Foundation of China (Nos. 21871105, 21975096, and 21501064). We thank the staff at BL17B1 beamline of the National Facility for Protein Science in Shanghai (NFPS), Shanghai Advanced Research Institute, Chinese Academy of Sciences (CAS), for providing technical support in X-ray diffraction data collection. We also thank Professor Rajamani Krishna from University of Amsterdam for the breakthrough calculations.

Electronic Supplementary Material: Supplementary material (synthetic procedures; ^{1}H nuclear magnetic resonance (NMR) spectra; single-crystal X-Ray diffraction data; structural models; FT-IR spectra; TGA curve; PXRD patterns in water and after N_2 sorption measurement; gas sorption isotherms at 273 K; the isosteric heats of adsorption; IAST selectivities for equimolar gas mixtures of C_3H_8/CH_4, C_2H_6/CH_4, C_2H_4/CH_4, C_2H_2/CH_4, CO_2/CH_4, C_2H_6/C_2H_4, C_2H_2/C_2H_4, and C_2H_2/CO_2 at 273 and 298 K respectively; comparison of C_3H_8 adsorption amounts at 0.05 bar and C_2H_6 adsorption amounts at 0.1 bar among representative MOFs; comparison of C_3H_8/CH_4 (5/85) and C_2H_6/CH_4 (10/85) selectivity with reported MOFs; comparison of C_3H_8/CH_4 (50/50) and C_2H_6/CH_4 (50/50) selectivity with representative MOFs; details of the numerical procedure used in breakthrough calculations) is available in the online version of this article at https://doi.org/10.1007/s12274-023-5634-x.

References

[1] Yaghi, O. M.; O'Keeffe, M.; Ockwig, N. W.; Chae, H. K.; Eddaoudi, M.; Kim, J. Reticular synthesis and the design of new materials. *Nature* **2003**, *423*, 705–714.

[2] Suh, M. P.; Park, H. J.; Prasad, T. K.; Lim, D. W. Hydrogen storage in metal-organic frameworks. *Chem. Rev.* **2012**, *112*, 782–835.

[3] Barnett, B. R.; Gonzalez, M. I.; Long, J. R. Recent progress towards light hydrocarbon separations using metal-organic frameworks. *Trends Chem.* **2019**, *1*, 159–171.

[4] Eddaoudi, M.; Kim, J.; Rosi, N.; Vodak, D.; Wachter, J.; O'Keeffe, M.; Yaghi, O. M. Systematic design of pore size and functionality in isoreticular MOFs and their application in methane storage. *Science* **2002**, *295*, 469–472.

[5] Freund, R.; Canossa, S.; Cohen, S. M.; Yan, W.; Deng, H. X.; Guillerm, V.; Eddaoudi, M.; Madden, D. G.; Fairen-Jimenez, D.; Lyu, H. et al. 25 years of reticular chemistry. *Angew. Chem., Int. Ed.* **2021**, *60*, 23946–23974.

[6] Ghasempour, H.; Wang, K. Y.; Powell, J. A.; ZareKarizi, F.; Lv, X. L.; Morsali, A.; Zhou, H. C. Metal-organic frameworks based on multicarboxylate linkers. *Coord. Chem. Rev.* **2021**, *426*, 213542.

[7] Chae, H. K.; Eddaoudi, M.; Kim, J.; Hauck, S. I.; Hartwig, J. F.; O'Keeffe, M.; Yaghi, O. M. Tertiary building units: Synthesis, structure, and porosity of a metal-organic dendrimer framework (MODF-1). *J. Am. Chem. Soc.* **2001**, *123*, 11482–11483.

[8] Øien-Ødegaard, S.; Shearer, G. C.; Wragg, D. S.; Lillerud, K. P. Pitfalls in metal-organic framework crystallography: Towards more accurate crystal structures. *Chem. Soc. Rev.* **2017**, *46*, 4867–4876.

[9] Cairns, A. B.; Goodwin, A. L. Structural disorder in molecular framework materials. *Chem. Soc. Rev.* **2013**, *42*, 4881–4893.

[10] Meekel, E. G.; Goodwin, A. L. Correlated disorder in metal-organic frameworks. *CrystEngComm* **2021**, *23*, 2915–2922.

[11] Chui, S. S. Y.; Lo, S. M. F.; Charmant, J. P. H.; Orpen, A. G.; Williams, I. D. A chemically functionalizable nanoporous material $[Cu_3(TMA)_2(H_2O)_3]_n$. *Science* **1999**, *283*, 1148–1150.

[12] Peng, Y.; Krungleviciute, V.; Eryazici, I.; Hupp, J. T.; Farha, O. K.; Yildirim, T. Methane storage in metal-organic frameworks: Current records, surprise findings, and challenges. *J. Am. Chem. Soc.* **2013**, *135*, 11887–11894.

[13] Wang, Q. M.; Shen, D. M.; Bülow, M.; Lau, M. L.; Deng, S. G.; Fitch, F. R.; Lemcoff, N. O.; Semanscin, J. Metallo-organic molecular sieve for gas separation and purification. *Micropor. Mesopor. Mater.* **2002**, *55*, 217–230.

[14] Spanopoulos, I.; Tsangarakis, C.; Klontzas, E.; Tylianakis, E.; Froudakis, G.; Adil, K.; Belmabkhout, Y.; Eddaoudi, M.; Trikalitis, P. N. Reticular synthesis of HKUST-like tbo-MOFs with enhanced CH_4 storage. *J. Am. Chem. Soc.* **2016**, *138*, 1568–1574.

[15] He, Y. B.; Krishna, R.; Chen, B. L. Metal-organic frameworks with potential for energy-efficient adsorptive separation of light hydrocarbons. *Energy Environ. Sci.* **2012**, *5*, 9107–9120.

[16] Mason, J. A.; Veenstra, M.; Long, J. R. Evaluating metal-organic frameworks for natural gas storage. *Chem. Sci.* **2014**, *5*, 32–51.

[17] Eubank, J. F.; Mouttaki, H.; Cairns, A. J.; Belmabkhout, Y.; Wojtas, L.; Luebke, R.; Alkordi, M.; Eddaoudi, M. The quest for modular nanocages: Tbo-MOF as an archetype for mutual substitution, functionalization, and expansion of quadrangular pillar building blocks. *J. Am. Chem. Soc.* **2011**, *133*, 14204–14207.

[18] Moreau, F.; Kolokolov, D. I.; Stepanov, A. G.; Easun, T. L.; Dailly, A.; Lewis, W.; Blake, A. J.; Nowell, H.; Lennox, M. J.; Besley, E. et al. Tailoring porosity and rotational dynamics in a series of octacarboxylate metal-organic frameworks. *Proc. Natl. Acad. Sci. USA* **2017**, *114*, 3056–3061.

[19] Chen, Y.; Wang, B.; Wang, X. Q.; Xie, L. H.; Li, J. P.; Xie, Y. B.; Li, J. R. A copper(II)-paddlewheel metal-organic framework with exceptional hydrolytic stability and selective adsorption and detection ability of aniline in water. *ACS Appl. Mater. Interfaces* **2017**, *9*, 27027–27035.

[20] Shao, K.; Wen, H. M.; Liang, C. C.; Xiao, X. Y.; Gu, X. W.; Chen, B. L.; Qian, G. D.; Li, B. Engineering supramolecular binding sites in a chemically stable metal-organic framework for simultaneous high C_2H_2 storage and separation. *Angew. Chem., Int. Ed.* **2022**, *61*,

e202211523.
[21] Shi, X. L.; Zu, Y. C.; Jiang, S. S.; Sun, F. X. An anionic indium-organic framework with spirobifluorene-based ligand for selective adsorption of organic dyes. *Inorg. Chem.* **2021**, *60*, 1571–1578.
[22] Feng, D. W.; Gu, Z. Y.; Li, J. R.; Jiang, H. L.; Wei, Z. W.; Zhou, H. C. Zirconium-metalloporphyrin PCN-222: Mesoporous metal-organic frameworks with ultrahigh stability as biomimetic catalysts. *Angew. Chem., Int. Ed.* **2012**, *51*, 10307–10310.
[23] Mondloch, J. E.; Bury, W.; Fairen-Jimenez, D.; Kwon, S.; DeMarco, E. J.; Weston, M. H.; Sarjeant, A. A.; Nguyen, S. T.; Stair, P. C.; Snurr, R. Q. et al. Vapor-phase metalation by atomic layer deposition in a metal-organic framework. *J. Am. Chem. Soc.* **2013**, *135*, 10294–10297.
[24] Jia, J. T.; Sun, F. X.; Fang, Q. R.; Liang, X. Q.; Cai, K.; Bian, Z.; Zhao, H. J.; Gao, L. X.; Zhu, G. S. A novel low density metal-organic framework with pcu topology by dendritic ligand. *Chem. Commun.* **2011**, *47*, 9167–9169.
[25] Saragi, T. P. I.; Spehr, T.; Siebert, A.; Fuhrmann-Lieker, T.; Salbeck, J. Spiro compounds for organic optoelectronics. *Chem. Rev.* **2007**, *107*, 1011–1065.
[26] Moreau, F.; Audebrand, N.; Poriel, C.; Moizan-Baslé, V.; Ouvry, J. A 9,9'-spirobifluorene based metal-organic framework: Synthesis, structure analysis and gas sorption properties. *J. Mater. Chem.* **2011**, *21*, 18715–18722.
[27] Park, H. J.; Jang, J. K.; Kim, S. Y.; Ha, J. W.; Moon, D.; Kang, I. N.; Bae, Y. S.; Kim, S.; Hwang, D. H. Synthesis of a Zr-based metal-organic framework with spirobifluorenetetrabenzoic acid for the effective removal of nerve agent simulants. *Inorg. Chem.* **2017**, *56*, 12098–12101.
[28] Fang, X. T.; Wang, L. Y.; He, X.; Xu, J. Q.; Duan, Z. M. A 3D calcium spirobifluorene metal-organic framework: Single-crystal-to-single-crystal transformation and toluene detection by a quartz crystal microbalance sensor. *Inorg. Chem.* **2018**, *57*, 1689–1692.
[29] Pang, J. D.; Wu, M. Y.; Qin, J. S.; Liu, C. P.; Lollar, C. T.; Yuan, D. Q.; Hong, M. C.; Zhou, H. C. Solvent-assisted, thermally triggered structural transformation in flexible mesoporous metal-organic frameworks. *Chem. Mater.* **2019**, *31*, 8787–8793.
[30] Hu, F. L.; Di, Z. Y.; Wu, M. Y.; Hong, M. C.; Li, J. A robust multifunctional Eu_6-cluster based framework for gas separation and recognition of small molecules and heavy metal ions. *Cryst. Growth Des.* **2019**, *19*, 6381–6387.
[31] Moreau, F.; Audebrand, N.; Poriel, C. 9,9'-Spirobifluorene based zinc coordination polymers: A study on linker geometry and topology. *CrystEngComm* **2020**, *22*, 293–303.
[32] Liu, Y.; Wang, J. M.; Imaz, I.; Maspoch, D. Assembly of colloidal clusters driven by the polyhedral shape of metal-organic framework particles. *J. Am. Chem. Soc.* **2021**, *143*, 12943–12947.
[33] Moghadam, P. Z.; Li, A.; Wiggin, S. B.; Tao, A. D.; Maloney, A. G. P.; Wood, P. A.; Ward, S. C.; Fairen-Jimenez, D. Development of a cambridge structural database subset: A collection of metal-organic frameworks for past, present, and future. *Chem. Mater.* **2017**, *29*, 2618–2625.
[34] Weber, J.; Antonietti, M.; Thomas, A. Microporous networks of high-performance polymers: Elastic deformations and gas sorption properties. *Macromolecules* **2008**, *41*, 2880–2885.
[35] Wu, C. Y.; Liu, Y. M.; Liu, H.; Duan, C. H.; Pan, Q. Y.; Zhu, J.; Hu, F.; Ma, X. Y.; Jiu, T. G.; Li, Z. B. et al. Highly conjugated three-dimensional covalent organic frameworks based on spirobifluorene for perovskite solar cell enhancement. *J. Am. Chem. Soc.* **2018**, *140*, 10016–10024.
[36] Modak, A.; Maegawa, Y.; Goto, Y.; Inagaki, S. Synthesis of 9,9'-spirobifluorene-based conjugated microporous polymers by $FeCl_3$-mediated polymerization. *Polym. Chem.* **2016**, *7*, 1290–1296.
[37] Zu, Y. C.; Li, J. W.; Li, X. L.; Zhao, T. Y.; Ren, H.; Sun, F. X. Imine-linked porous aromatic frameworks based on spirobifluorene building blocks for CO_2 separation. *Micropor. Mesopor. Mater.* **2022**, *334*, 111779.
[38] Suresh, K.; Kalenak, A. P.; Sotuyo, A.; Matzger, A. J. Metal-organic framework (MOF) morphology control by design. *Chem. —Eur. J.* **2022**, *28*, e202200334.
[39] Cayron, C. Multiple twinning in cubic crystals: Geometric/algebraic study and its application for the identification of the $\Sigma 3^n$ grain boundaries. *Acta Crystallogr. A* **2007**, *63*, 11–29.
[40] Hadjiivanov, K. I.; Panayotov, D. A.; Mihaylov, M. Y.; Ivanova, E. Z.; Chakarova, K. K.; Andonova, S. M.; Drenchev, N. L. Power of infrared and Raman spectroscopies to characterize metal-organic frameworks and investigate their interaction with guest molecules. *Chem. Rev.* **2021**, *121*, 1286–1424.
[41] Sahoo, R.; Das, M. C. C_{2s}/C_1 hydrocarbon separation: The major step towards natural gas purification by metal-organic frameworks (MOFs). *Coord. Chem. Rev.* **2021**, *442*, 213998.
[42] Dincă, M.; Dailly, A.; Liu, Y.; Brown, C. M.; Neumann, D. A.; Long, J. R. Hydrogen storage in a microporous metal-organic framework with exposed Mn^{2+} coordination sites. *J. Am. Chem. Soc.* **2006**, *128*, 16876–16883.
[43] Sumida, K.; Rogow, D. L.; Mason, J. A.; McDonald, T. M.; Bloch, E. D.; Herm, Z. R.; Bae, T. H.; Long, J. R. Carbon dioxide capture in metal-organic frameworks. *Chem. Rev.* **2012**, *112*, 724–781.
[44] Gao, S.; Morris, C. G.; Lu, Z. Z.; Yan, Y.; Godfrey, H. G. W.; Murray, C.; Tang, C. C.; Thomas, K. M.; Yang, S. H.; Schröder, M. Selective hysteretic sorption of light hydrocarbons in a flexible metal-organic framework material. *Chem. Mater.* **2016**, *28*, 2331–2340.
[45] Bloch, E. D.; Queen, W. L.; Krishna, R.; Zadrozny, J. M.; Brown, C. M.; Long, J. R. Hydrocarbon separations in a metal-organic framework with open iron(II) coordination sites. *Science* **2012**, *335*, 1606–1610.
[46] He, Y. B.; Zhang, Z. J.; Xiang, S. C.; Fronczek, F. R.; Krishna, R.; Chen, B. L. A robust doubly interpenetrated metal-organic framework constructed from a novel aromatic tricarboxylate for highly selective separation of small hydrocarbons. *Chem. Commun.* **2012**, *48*, 6493–6495.
[47] Zhang, Y. B.; Yang, L. F.; Wang, L. Y.; Cui, X. L.; Xing, H. B. Pillar iodination in functional boron cage hybrid supramolecular frameworks for high performance separation of light hydrocarbons. *J. Mater. Chem. A* **2019**, *7*, 27560–27566.
[48] Plonka, A. M.; Chen, X. Y.; Wang, H.; Krishna, R.; Dong, X. L.; Banerjee, D.; Woerner, W. R.; Han, Y.; Li, J.; Parise, J. B. Light hydrocarbon adsorption mechanisms in two calcium-based microporous metal organic frameworks. *Chem. Mater.* **2016**, *28*, 1636–1646.
[49] Chen, Y. L.; Bai, X. Y.; Liu, D. H.; Fu, X. L.; Yang, Q. Y. High-throughput computational exploration of MOFs with open Cu sites for adsorptive separation of hydrogen isotopes. *ACS Appl. Mater. Interfaces* **2022**, *14*, 24980–24991.
[50] Ponraj, Y. K.; Borah, B. High-throughput computational screening of metal-organic frameworks for the separation of methane from ethane and propane. *J. Phys. Chem. C* **2021**, *125*, 1839–1854.
[51] Yang, S. Q.; Hu, T. L. Reverse-selective metal-organic framework materials for the efficient separation and purification of light hydrocarbons. *Coord. Chem. Rev.* **2022**, *468*, 214628.
[52] Cheng, H. T.; Wang, Q.; Meng, L. L.; Sheng, P.; Zhang, Z. H.; Ding, M.; Gao, Y. J.; Bai, J. F. Formation of a N/O/F-rich and rooflike cluster-based highly stable Cu(I/II)-MOF for promising pipeline natural gas upgrading by the recovery of individual C_3H_8 and C_2H_6 gases. *ACS Appl. Mater. Interfaces* **2021**, *13*, 40713–40723.
[53] Zhou, J. Y.; Ke, T.; Steinke, F.; Stock, N.; Zhang, Z. G.; Bao, Z. B.; He, X.; Ren, Q. L.; Yang, Q. W. Tunable confined aliphatic pore environment in robust metal-organic frameworks for efficient separation of gases with a similar structure. *J. Am. Chem. Soc.* **2022**, *144*, 14322–14329.
[54] Jia, J. T.; Wang, L.; Sun, F. X.; Jing, X. F.; Bian, Z.; Gao, L. X.; Krishna, R.; Zhu, G. S. The adsorption and simulated separation of light hydrocarbons in isoreticular metal-organic frameworks based on dendritic ligands with different aliphatic side chains. *Chem. —Eur. J.* **2014**, *20*, 9073–9080.
[55] Zhang, Y. F.; Xiao, H. Y.; Zhou, X.; Wang, X.; Li, Z. Selective adsorption performances of UiO-67 for separation of light hydrocarbons C1, C2, and C3. *Ind. Eng. Chem. Res.* **2017**, *56*, 8689–8696.
[56] Huang, Y. B.; Lin, Z. J.; Fu, H. R.; Wang, F.; Shen, M.; Wang, X. S.; Cao, R. Porous anionic indium-organic framework with enhanced gas and vapor adsorption and separation ability. *ChemSusChem*

2014, *7*, 2647–2653.
[57] Wang, D. M.; Zhang, J.; Li, G. H.; Yuan, J. Q.; Li, J. T.; Huo, Q. S.; Liu, Y. L. Mesoporous hexanuclear copper cluster-based metal-organic framework with highly selective adsorption of gas and organic dye molecules. *ACS Appl. Mater. Interfaces* **2018**, *10*, 31233–31239.
[58] Liu, H.; Li, B. R.; Zhao, Y. Y.; Kong, C. L.; Zhou, C.; Lin, Y. C.; Tian, Z. Q.; Chen, L. Investigation on a Zr-based metal-organic framework (MOF-801) for the high-performance separation of light alkanes. *Chem. Commun.* **2021**, *57*, 13008–13011.
[59] Li, L.; Wang, X. S.; Liang, J.; Huang, Y. B.; Li, H. F.; Lin, Z. J.; Cao, R. Water-stable anionic metal-organic framework for highly selective separation of methane from natural gas and pyrolysis gas. *ACS Appl. Mater. Interfaces* **2016**, *8*, 9777–9781.
[60] Liu, B.; Yao, S.; Shi, C.; Li, G. H.; Huo, Q. S.; Liu, Y. L. Significant enhancement of gas uptake capacity and selectivity via the judicious increase of open metal sites and Lewis basic sites within two polyhedron-based metal-organic frameworks. *Chem. Commun.* **2016**, *52*, 3223–3226.
[61] Zhang, Y. B.; Yang, L. F.; Wang, L. Y.; Duttwyler, S.; Xing, H. B. A microporous metal-organic framework supramolecularly assembled from a Cu^{II} dodecaborate cluster complex for selective gas separation. *Angew. Chem., Int. Ed.* **2019**, *58*, 8145–8150.
[62] Sun, Q. S.; Yao, S.; Liu, B.; Liu, X. Y.; Li, G. H.; Liu, X. Y.; Liu, Y. L. A novel polyhedron-based metal-organic framework with high performance for gas uptake and light hydrocarbon separation. *Dalton Trans.* **2018**, *47*, 5005–5010.
[63] Yuan, Y. N.; Wu, H. X.; Xu, Y. Z.; Lv, D. F.; Tu, S.; Wu, Y.; Li, Z.; Xia, Q. B. Selective extraction of methane from C1/C2/C3 on moisture-resistant MIL-142A with interpenetrated networks. *Chem. Eng. J.* **2020**, *395*, 125057.
[64] Guo, P. T.; Chang, M.; Yan, T. G.; Li, Y. X.; Liu, D. H. A pillared-layer metal-organic framework for efficient separation of $C_3H_8/C_2H_6/CH_4$ in natural gas. *Chin. J. Chem. Eng.* **2022**, *42*, 10–16.
[65] Ding, M.; Wang, Q.; Cheng, H. T.; Bai, J. F. Synthesis, structure and highly selective C_3H_8/CH_4 and C_2H_6/CH_4 adsorption of a (4,8)-c ternary *flu*-metal-organic framework based upon both $[Sc_4O_2(COO)_8]$ and $[Cu_4OCl_6]$ clusters. *CrystEngComm* **2022**, *24*, 2388–2392.
[66] Belmabkhout, Y.; Mouttaki, H.; Eubank, J. F.; Guillerm, V.; Eddaoudi, M. Effect of pendant isophthalic acid moieties on the adsorption properties of light hydrocarbons in HKUST-1-like tbo-MOFs: Application to methane purification and storage. *RSC Adv.* **2014**, *4*, 63855–63859.
[67] Krishna, R. The maxwell-stefan description of mixture diffusion in nanoporous crystalline materials. *Microporous Mesoporous Mater.* **2014**, *185*, 30–50.
[68] Krishna, R. Methodologies for evaluation of metal-organic frameworks in separation applications. *RSC Adv.* **2015**, *5*, 52269–52295.
[69] Krishna, R. Screening metal-organic frameworks for mixture separations in fixed-bed adsorbers using a combined selectivity/capacity metric. *RSC Adv.* **2017**, *7*, 35724–35737.
[70] Krishna, R. Methodologies for screening and selection of crystalline microporous materials in mixture separations. *Sep. Purif. Technol.* **2018**, *194*, 281–300.
[71] Krishna, R. Metrics for evaluation and screening of metal-organic frameworks for applications in mixture separations. *ACS Omega* **2020**, *5*, 16987–17004.